Extreme chirality in Swiss roll metamaterials



2009 J. Phys.: Condens. Matter 21 376003

(http://iopscience.iop.org/0953-8984/21/37/376003)

J. Phys.: Condens. Matter **21** (2009) 376003 (8pp) doi:10.1088/0953-8984/21/37/376003

# Extreme chirality in Swiss roll metamaterials

**A Demetriadou and J B Pendry**

The Blackett Laboratory, Imperial College, London SW7 2AZ, UK

E-mail: ademetri@imperial.ac.uk and j.pendry@imperial.ac.uk

Received 16 February 2009, in final form 31 July 2009
Published 19 August 2009
Online at stacks.iop.org/JPhysCM/21/376003

**Abstract**
The chiral Swiss roll metamaterial is a resonant, magnetic medium that exhibits a negative refractive band for one-wave polarization. Its unique structure facilitates huge chiral effects: a plane polarized wave propagating through this system can change its polarization by 90° in less than a wavelength. Such chirality is at least 100 times greater than previous structures have achieved. In this paper, we discuss this extreme chiral behaviour with both numerical and analytical results.

(Some figures in this article are in colour only in the electronic version)

## 1. Introduction

It is well known that the electromagnetic response of conventional materials is dependent on their molecular composition and usually have both/either the electric permittivity ($\varepsilon$) and/or the magnetic permeability ($\mu$) positive. Since the structure and composition of molecules and atoms are rather restrictive, the electromagnetic properties of conventional media are limited. In the past few years, new artificial media, called metamaterials, have been developed that are capable of overcoming these restrictions. Metamaterials' subunits are much smaller than the wavelength of incident radiation, such that an incident wave sees a homogeneous medium and not the geometry of the subunits. Therefore, the subunit of a metamaterial can be specifically designed to manufacture media with advantageous and novel electromagnetic properties, such as negative refraction and perfect lensing.

Although negative refraction is a property not found in nature, Veselago, in 1968 [1], by considering causality and dispersion for real media and the fact that from Maxwell's equations the refractive index ($n$) is given by $n = \sqrt{\varepsilon(\omega)\mu(\omega)}$, pointed out that materials with $\mathrm{Re}(\varepsilon(\omega))$ and $\mathrm{Re}(\mu(\omega))$ simultaneously negative, exhibit a negative refractive index. However, considering that the imaginary parts of $\varepsilon(\omega)$ and $\mu(\omega)$ are restricted to be positive and related to the real parts by the Kramer–Kronig relations, the refractive index can be rewritten as:

$$n = \begin{cases} +\sqrt{\varepsilon(\omega)\mu(\omega)} & \text{for } \mathrm{Re}(\varepsilon) > 0 \text{ and } \mathrm{Re}(\mu) > 0 \\ -\sqrt{\varepsilon(\omega)\mu(\omega)} & \text{for } \mathrm{Re}(\varepsilon) < 0 \text{ and } \mathrm{Re}(\mu < 0). \end{cases} \quad (1)$$

The most well-known negatively-refractive metamaterial is constructed by combining an artificial plasma (such as a wire mesh metamaterial [2–4]), and a magnetic resonator (for example split ring resonators [5]), providing the negative permittivity ($\mathrm{Re}(\varepsilon) < 0$) and negative permeability ($\mathrm{Re}(\mu) < 0$) respectively. These metamaterials are usually called doubly negative metamaterials, since two different resonant structures are combined to provide a negative refractive index over a frequency range, as shown in figure 1. However, their applications are considerably limited due to resonance losses and the difficulty of manufacturing an artificial magnetic structure for high frequencies. Also, their band structure is not continuous at the transition from the negative to positive band (figure 1) [6].

Based on the above observations, several alternative metamaterial structures were introduced in the literature that also support negative refraction and avoid some of these problems. Chiral media are an example, since they exhibit a backward wave without requiring both $\varepsilon$ and $\mu$ to be negative [6–10]. Generally a structure is said to be chiral if it is not identical to its mirror image and chirality in a medium leads to the macroscopic rotation of the wave polarization. Hence, the electromagnetic fields in a chiral medium can be written

 

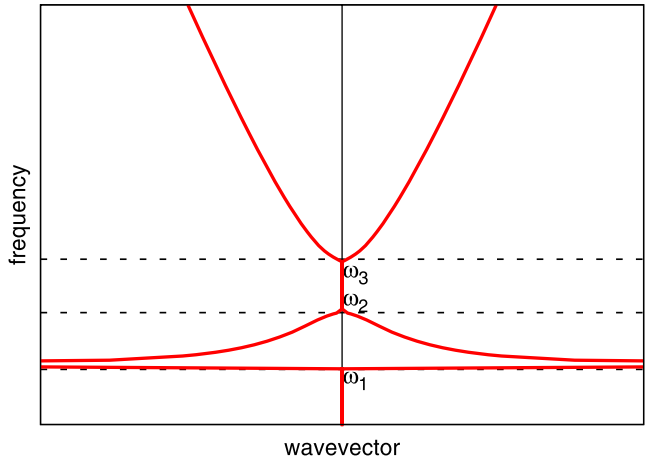


**Figure 1.** The band structure of a typical doubly negative metamaterial, consisted from a wire mesh and split ring resonators, where $\omega_1$ is the resonant frequency of the split ring resonators, $\omega_2$ is the magnetic plasma frequency of the split ring resonators and $\omega_3$ is the plasma frequency of the wire mesh.

as [6]:

$$\begin{bmatrix} \mathbf{D} \\ \mathbf{B} \end{bmatrix} = \begin{bmatrix} \chi_{EE} & \chi_{EH} \\ \chi_{HE} & \chi_{HH} \end{bmatrix} \begin{bmatrix} \mathbf{E} \\ \mathbf{H} \end{bmatrix} \tag{2}$$

where **D** is the electric displacement vector, **E** the electric field intensity, **B** is the magnetic induction field and **H** the magnetic field intensity. The parameters $\chi_{EE}$ and $\chi_{HH}$ are the electric permittivity and magnetic permeability of the medium, respectively, and $\chi_{EH}$ and $\chi_{HE}$ are the chirality parameters. As described in [6], a dipole medium (electric or magnetic) exhibits two degenerate modes and a stop-band for frequencies where $\varepsilon$ or $\mu$ is negative. Now, if chiral inclusions are introduced to this medium, the degenerate modes split, resulting in a negative band for one of the wave polarizations [6]. Therefore, chiral metamaterials can achieve negative refraction with a continuous transition between the negative and the positive bands, requiring just one resonant structure. Here, it is worth mentioning that chiral inclusions of aligned handedness ensure macroscopically rotatory power. If half of them have opposite handedness, the rotatory power disappears [11]. Examples of chiral metamaterials are helical-shaped conducting wires [10, 12] and chiral Swiss rolls [6]. In this paper the chiral Swiss roll metamaterial is discussed and is shown that it exhibits an enormous chirality compared with other structures in literature.

Initially let us consider briefly the simple case of the non-chiral Swiss roll metamaterial, shown in figure 2(a). A non-chiral Swiss roll resonator is made of a conducting sheet, arranged in a spiral shape and it demonstrates a macroscopic magnetic behaviour [5]. For a magnetic field applied along the rod, currents are induced on the spiral conducting sheet, which in their turn give rise to an electromotive force (emf) opposing the applied magnetic field. Therefore, it appears macroscopically that 'magnetic monopoles' are flowing up and down the rod [5, 13], creating a magnetic equivalent of the parallel-wire structure. The effective magnetic permeability of the Swiss roll metamaterial (with the rods aligned with $z$-axes) is given by [5]:

$$\mu_z = 1 - \frac{F\omega^2}{\omega^2 - \omega_0^2 + \mathrm{i}\Gamma\omega} \tag{3}$$

where $F = \pi R^2/a^2$ is the filling factor and the resonant frequency is given by:

$$\omega_0^2 = \frac{dc_0^2}{2\pi^2 R^3 \varepsilon_d (N-1)} \tag{4}$$

where $R$ is the outer radius, $a$ the lattice constant, $\varepsilon_d$ is the dielectric permittivity of the material in the gap, $d$ is the gap between the conducting sheets, $\Gamma = 2\rho/[\mu_0 R(N-1)]$ accounts for the resistivity losses of the conducting material [5] and $\rho$ is the resistance of the roll per unit area. The magnetic permeability is zero at $\omega_{\mathrm{mp}}$ and the 'magnetic' plasma frequency is given by [5]:

$$\omega_{\mathrm{mp}}^2 = \frac{dc_0^2}{(1-F)2\pi^2 R^3 \varepsilon_d (N-1)} = \frac{\omega_0^2}{(1-F)}. \tag{5}$$

A non-chiral Swiss roll metamaterial, with the rods arranged in a square lattice and all aligned with the $z$-axes has a band structure given by [14, 15]:

$$\omega = c_0 \sqrt{\frac{k_x^2}{\varepsilon_y \mu_z} + \frac{k_z^2}{\varepsilon_y \mu_x}} \tag{6}$$

and plotted in figure 2(b) for $k_x$-propagation (i.e. $k_y = k_z = 0$) [16, 14]. Note that there is stop-band for frequencies where $\mu_z$ is negative ($\omega_0 < \omega < \omega_{\mathrm{mp}}$). In this paper, we discuss the chiral Swiss roll structure by investigating its electromagnetic and chiral behaviour, both numerically and analytically. Also, the band structure of the chiral metamaterial is calculated numerically and compared with previous analytical work in [6]. Finally the electromagnetic and chiral parameters are derived and compared with other chiral structures in recent literature.

## 2. Electromagnetic and chirality parameters

A chiral Swiss roll can be constructed by winding an insulated conducting sheet (of the shape shown in figure 3(a)), around a cylindrical mandrel, creating an overlapping helix. Each layer of the conducting sheet is separated by distance $d$, filled with air or a dielectric material of $\varepsilon_d$ and $N$ is the number of turns measured at a cross section. The external radius of the rod is $R$ and the structure has periodicity $p = 2\pi R \tan\theta$, width $w = 2\pi RN \sin\theta$ and the length of the conducting foil is $l = N\pi R \sin 2\theta$. The structure has a magnetic resonance, arising in the same way as for the non-chiral Swiss roll, described above. However, its helical shape provides the chirality of the structure [6].

In order to derive the electromagnetic and chirality parameters of the chiral Swiss roll, let us consider uniform fields $H_z$ and $E_z$, applied along a right-handed chiral Swiss roll. The $H_z$-field induces a current flowing in the $x$–$y$ plane. $E_z$ creates charge accumulation at the edges of the foil, since

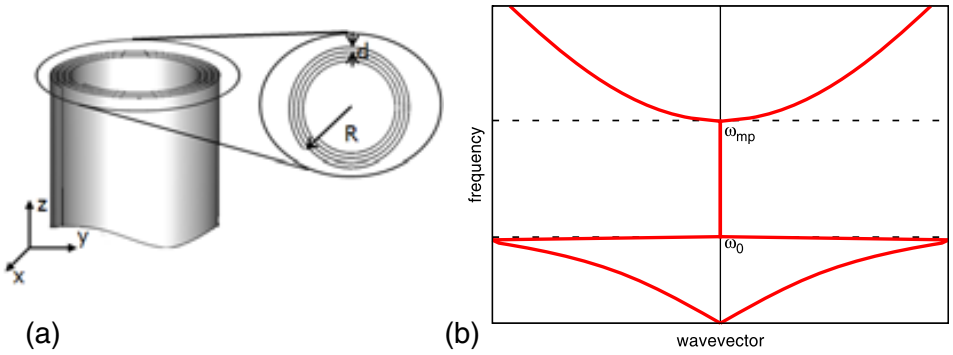


**Figure 2.** (a) A non-chiral Swiss roll, where $R$ is the outer radius, $d$ is the gap between the conducting sheets. (b) The analytical prediction for the band structure of a Swiss roll for $k_x$ propagation. A stop-band is expected for frequencies where $\mu_z$ is negative (i.e. $\omega_0 < \omega < \omega_{mp}$).

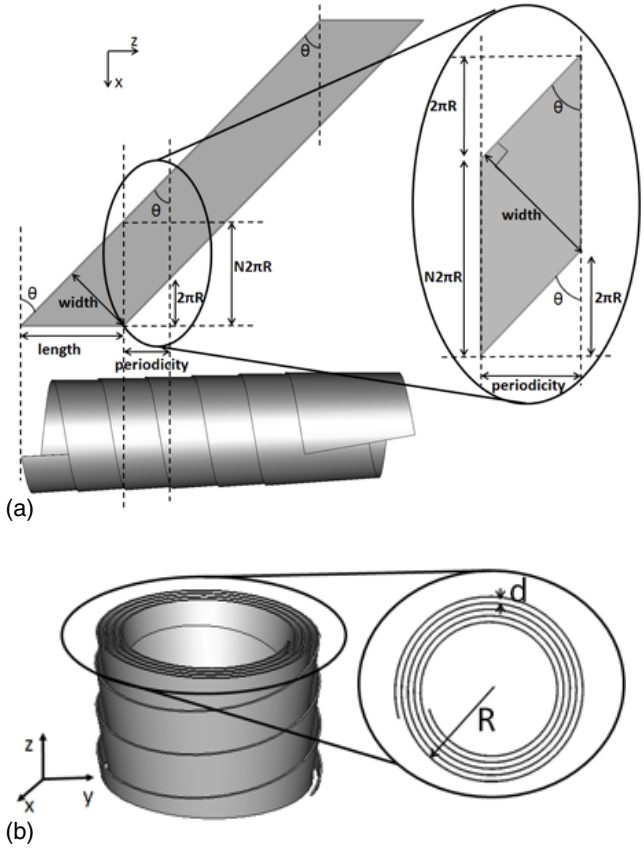


**Figure 3.** (a) The (unfolded) conducting sheet used to create a right-handed chiral Swiss roll. When wrapped around a cylindrical mandrel, a helical conducting structure is created. The enlarged part is the unfolded section of the foil that when wrapped gives the unit cell of a chiral Swiss roll. (b) The cross section of a chiral Swiss roll, where $R$ is the radius and $d$ the gap between the conducting sheet.

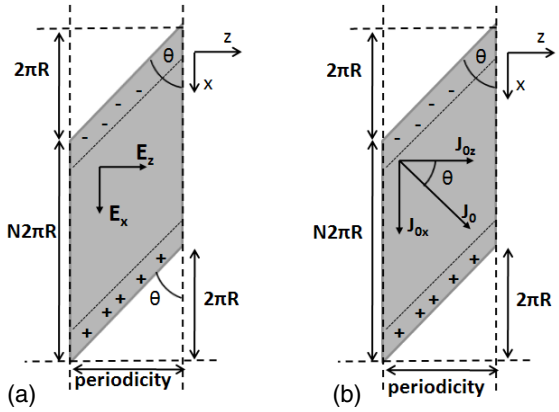


**Figure 4.** The periodic element of a chiral Swiss roll unwrapped. The dotted lines on the unfolded sheet show the exposed part of the conducting foil to either the inside or outside of the chiral Swiss roll. (a) The electric field due to charge accumulation at the edges of the conducting sheet, resolved in $x$- and $z$-components. (b) The current $\mathbf{J_0}$ is perpendicular to the edges of the foil and is dependent on charge accumulation at the edges.

it is not continuous (along the $z$-axis), giving rise to an electric field perpendicular to the edges of the conducting sheet (shown in figure 4(a) resolved to $x$- and $z$-components). Also, keep in mind that the edges of the conducting foil are exposed either outside or inside the rod and are shown in figure 4 with dashed lines.

Assuming that there are no local field effects, the cylinder has rotational symmetry and the current varies only across the width of the conducting sheet. Also, since the foil within the dashed lines is not exposed to either the outside or inside of the chiral Swiss roll, $\mathbf{J_0}$ is constant in magnitude and direction, and can be written as: $\mathbf{J_0} = \mathbf{J_{0x}} \sin\theta + \mathbf{J_{0z}} \cos\theta$, where $\mathbf{J_0}$ is the current perpendicular to the edges of the unfolded conducting sheet (figure 4(b)). Furthermore, if we assume a small gap between the conducting sheet (i.e. $R \gg d$) and a large number of turns ($N$), a large overlap of the conducting sheet is ensured. Now by considering the magnetic field along the $z$-axis (i.e. $H_z$), the potential difference and the charging of the capacitor between the inner and outer exposed foil and finally the emf arising from the induced current, the inverse electromagnetic and chirality parameters can be obtained (for a detailed derivation see appendix A):

$$[\chi^{-1}]_{HH} = \frac{1}{(1-F)}\left(\frac{\omega^2 - \omega_0^2 + \mathrm{i}\Gamma\omega}{\omega^2 - \omega_{\mathrm{mp}}^2 + \mathrm{i}\Gamma\omega/(1-F)}\right) \tag{7}$$

$$[\chi^{-1}]_{EE} = G\left(\frac{\omega^2 + \mathrm{i}\omega\Gamma/(1-F)}{\omega^2 - \omega_{\mathrm{p}}^2 + \mathrm{i}\omega\Gamma/(1-F)}\right) \tag{8}$$

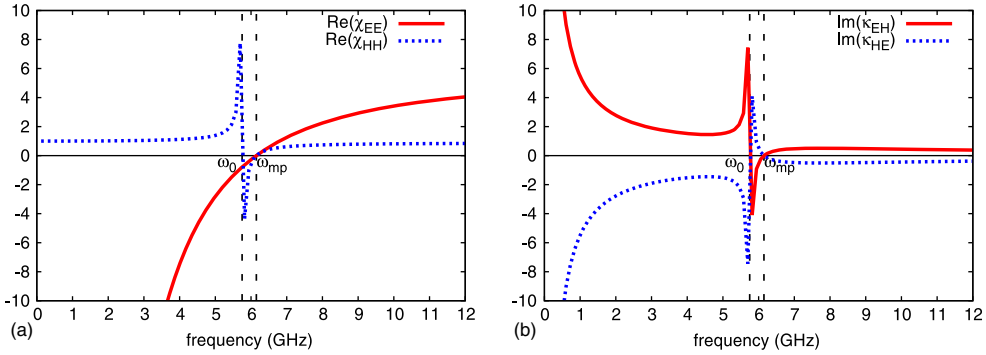


**Figure 5.** For Swiss rolls of $N = 2$, $R = 1$ mm, $l = 5$ mm, $x = 0.05$ mm, $d = 0.35$ mm, $\theta = 21, 7°$ and $a = 5$ mm. (a) The magnetic permeability ($\chi_{HH}$) is plotted with the red line and the electric permittivity tensor ($\chi_{EE}$) with the blue line. (b) The chirality terms ($\kappa_{EH}$ and $\kappa_{HE}$), which are equal and opposite (i.e. $\kappa_{EH} = -\kappa_{HE}$).

$$[\chi^{-1}]_{HE}/\varepsilon_0 = -\frac{\mathrm{i}R}{2L\tan\theta}\left(\frac{\omega_{\mathrm{mp}}^2\omega}{\omega^2 - \omega_{\mathrm{mp}}^2 + \mathrm{i}\Gamma\omega/(1-F)}\right) = [\kappa^{-1}]_{HE} \tag{9}$$

$$[\chi^{-1}]_{EH}/\mu_0 = \frac{\mathrm{i}R}{2L\tan\theta}\left(\frac{\omega\omega_{\mathrm{mp}}^2}{\omega^2 - \omega_{\mathrm{mp}}^2 + \mathrm{i}\Gamma\omega/(1-F)}\right) = [\kappa^{-1}]_{EH} \tag{10}$$

where $\chi^{-1}$ are the elements from the inverse tensor of (2), $\chi_{EE}$ the electric permittivity, $\chi_{HH}$ the magnetic permeability, $\chi_{EH}$ and $\chi_{HE}$ the chirality parameters (note that $F = \pi R^2/a^2$ is the filling factor, $[\kappa^{-1}]_{EH} = -[\kappa^{-1}]_{HE}$). Additionally, $\omega$ is the frequency, $R$, $\theta$ and $d$ are the dimensions of the chiral Swiss roll as defined in figure 3(a), $a$ the lattice constant and $G$ is a constant given by:

$$G = \frac{a^2 d}{L(8\pi^3 R^3(N-1)L\tan^2\theta + a^2 d)} \tag{11}$$

and

$$L = 1 - \omega\frac{\mathrm{i}\varepsilon_d\varepsilon_0 a^2\rho}{2\pi R}. \tag{12}$$

Furthermore,

$$\Gamma = -\frac{2\rho}{\mu_0 R} \tag{13}$$

accounts for the resistivity losses in the conducting sheet and $\rho$ is the resistance of the roll per unit area. Note that the resistivity losses for microwave frequencies are negligible, compared to the lossy character of the dielectric in the gap. The resonant frequencies $\omega_0$, $\omega_{\mathrm{mp}}$ and $\omega_{\mathrm{p}}$ are the given by:

$$\omega_0 = c_0\sqrt{\frac{4\pi L d\tan^2\theta}{\varepsilon_d(8(N-1)L\pi^3R^3\tan^2\theta + a^2 d)}}. \tag{14}$$

The magnetic and electric plasma frequencies take the same values and are given by:

$$\omega_{\mathrm{mp}} = \frac{\omega_0}{\sqrt{1-F}} = \omega_{\mathrm{p}}. \tag{15}$$

The electromagnetic parameters are plotted in figure 5 for a chiral Swiss roll with dimensions $N = 2$, $R = 1$ mm, $l = 5$ mm, $d = 0.35$ mm, $\theta = 21, 7°$, $a = 5$ mm and thickness of conducting sheet $x = 0.05$ mm. Note that both $\chi_{EE}$ and $\chi_{HH}$ are zero at the same frequency, since $\omega_{\mathrm{mp}} = \omega_{\mathrm{p}}$ and both $\chi_{EE}$ and $\chi_{HH}$ are negative for frequencies $\omega_0 < \omega < \omega_{\mathrm{mp}}$ as expected. Also, the chirality terms take infinite values for $\omega \to \omega_0$ and zero value for $\omega_{\mathrm{mp}}$. Finally, note that both $\chi_{HH}$ in (7) and $\mu_z$ in (3) obey the Lorentz model, since the magnetic behaviour of both structures arises from the same mechanism.

## 3. Band structure

A 2D chiral medium can be constructed by alternating the alignment of neighbouring layers of chiral Swiss rolls, as shown in figure 6(a). If the Swiss rolls are aligned with the $y$- and $z$-axes, then, the fields are given by (2), for propagation along the $x$-axes (i.e. $k_y = k_z = 0$). Also, now (7)–(10), are valid for electric and magnetic fields along both the $y$- ans $z$-axes. Using, Maxwell's equations and helical polarization for the electric and magnetic fields, the dispersion equations can be derived (explained in greater detail in [6]):

$$\omega^{+\pm} = c_0 k_{+\pm}\left(\mathrm{i}[\kappa^{-1}]_{EH}/c_0 \pm \sqrt{[\chi^{-1}]_{EE}[\chi^{-1}]_{HH}}\right) \tag{16}$$

$$\omega^{-\pm} = c_0 k_{-\pm}\left(-\mathrm{i}[\kappa^{-1}]_{EH}/c_0 \pm \sqrt{[\chi^{-1}]_{EE}[\chi^{-1}]_{HH}}\right) \tag{17}$$

for the positive and negative polarizations respectively and where $[\kappa^{-1}]_{EH}$, $[\chi^{-1}]_{EE}$ and $[\chi^{-1}]_{HH}$ are the inverse chirality, electric and magnetic parameters respectively.

Using (7)–(10), the band structure for a 2D chiral Swiss roll medium can be plotted, and is shown in figures 6(b) and (c) with full lines, for the real and imaginary part respectively. As it was expected, the degeneracy of the modes no longer holds, since the chirality splits the two modes and a negative band for one-wave polarization has emerged for frequencies $\omega_0 < \omega < \omega_{\mathrm{mp}}$. Also, for frequencies $\omega < \omega_0$, there is a stop-band as expected, since $\chi_{EE}$ is negative and $\chi_{HH}$ is positive. Finally, the wavevector (i.e. $\Delta k$) at which the frequency takes the minimum value is dependent on the resonant frequency ($\omega_0$) and the inverse chirality at the resonant frequency ($[\kappa^{-1}]_{EH}(\omega_0)$) and is given by:

$$\Delta k = \pm\frac{\omega_0}{\mathrm{Im}([\kappa^{-1}]_{EH}(\omega_0))}. \tag{18}$$

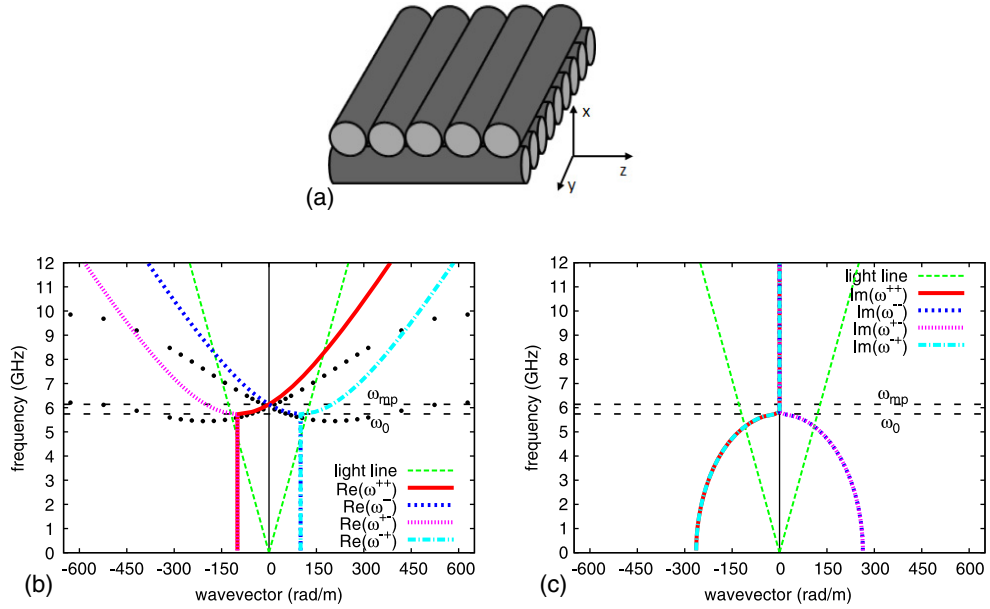


**Figure 6.** (a) Chiral Swiss rolls are placed along the $y$- and $z$-axes, creating a 2D chiral Swiss roll metamaterial. (b) The analytic prediction for the band structure of a 2D chiral Swiss roll metamaterial is shown with full lines and the numerical results with dots for dimensions $N = 2$, $R = 1$ mm, $l = 5$ mm, $x = 0.05$ mm, $d = 0.35$ mm, $\theta = 21, 7°$ and $a = 5$ mm. (c) The analytic prediction for the imaginary wavevector.

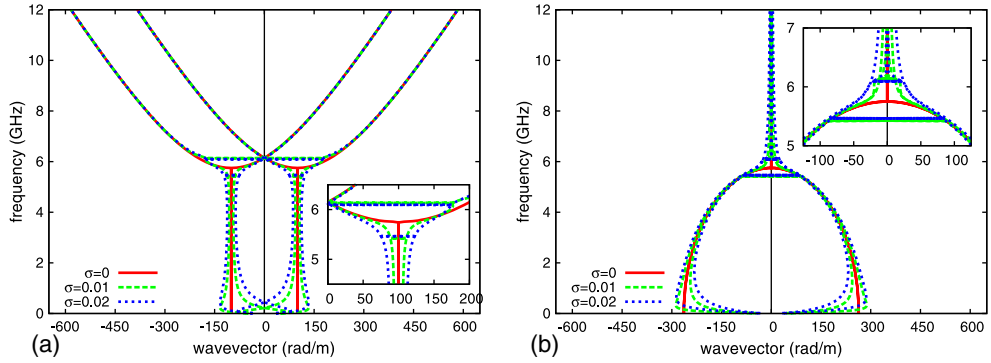


**Figure 7.** The band structure (a) real part, (b) imaginary part of 2D Swiss roll metamaterial for various values of $\sigma$ and with dimensions $N = 2$, $R = 1$ mm, $l = 5$ mm, $x = 0.05$ mm, $d = 0.35$ mm, $\theta = 21, 7°$ and $a = 5$ mm. Red solid line: $\sigma = 0$-vacuum, green dashed line: $\sigma = 0.01$ and blue dotted line: $\sigma = 0.02$.

Using CST Microwave studio, the band structure of a 2D chiral Swiss roll medium (as shown in figure 6(a)), with dimensions $N = 2$, $R = 1$ mm, $l = 5$ mm, $x = 0.05$ mm, $d = 0.35$ mm, $\theta = 21, 7°$ and $a = 5$ mm was calculated and is plotted in figure 6(b) (dots) with the analytical dispersion equations (full lines) shown in (16) and (17). The two band structures have a similar shape, with a negative band corresponding to one-wave polarization. The agreement between the analytical and the numerical calculations for the resonant frequencies is approximately ∼80% and for $\Delta k$ is ∼84%. Considering that the analytical prediction for this structure was derived assuming that $N$ is large, $R \gg d$ and an infinitely thin conducting sheet (which are not precisely valid for the chiral Swiss roll considered numerically), the agreement between the analytical and numerical results is significant.

Losses in Swiss roll metamaterials are mainly due to the dielectric material in the gap. In order to take them into account, just consider a complex $\varepsilon_d$ given by:

$$\varepsilon_d = \varepsilon' + \mathrm{i}\varepsilon'' = \varepsilon' + \mathrm{i}\frac{\sigma}{\omega\varepsilon_0} \tag{19}$$

where $\sigma$ is the conductivity of the dielectric. In figure 7, the band structure is plotted for various values of $\sigma$. For large enough $\sigma$ the modes do not meet at $\Delta k$. In figure 8, the band structure of a 2D Swiss roll metamaterials is plotted which has vacuum in the gap (red solid line) and a dielectric materials of $\sigma = 0.0167$ (blue dotted line). The bands slightly shift towards lower frequencies. Resistivity losses of metals for GHz and MHz frequencies that Swiss rolls operate, are negligibly small (i.e. for copper resistivity $\sim 1.7 \times 10^{-8}$). Figure 9, the band structure for various metals with difference resistivity. It is clear that resistance losses are insignificant at this frequency range.

Swiss rolls are most commonly used in the MHz frequency range [17, 14]. MHz-Swiss rolls are complex

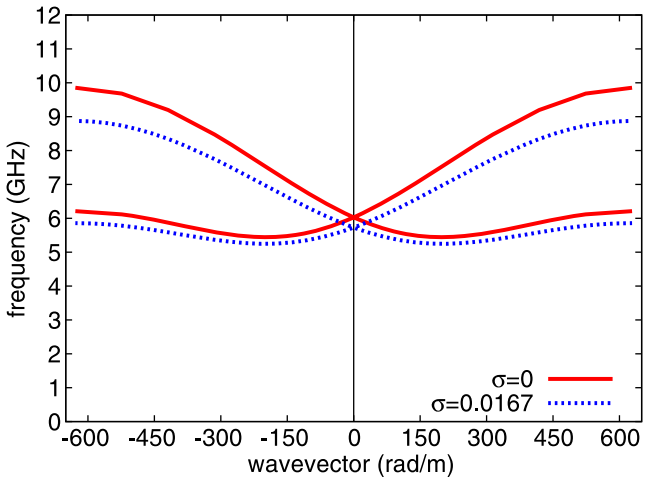


**Figure 8.** The band structure of Swiss rolls with dimensions $N = 2$, $R = 1$ mm, $l = 5$ mm, $x = 0.05$ mm, $d = 0.35$ mm, $\theta = 21, 7°$ and $a = 5$ mm. Red solid line for vacuum (i.e. $\sigma = 0$) between the conducting sheets and blue dotted line of $\sigma = 0.0167$.

structures, with extremely fine details demanding an enormous computational time in order to be modelled with today's computer capabilities. Therefore, a structure with smaller $N$, bigger $d$ and $\theta$ was simulated in order to investigate the structure numerically. Nevertheless, since there is a good agreement for a structure with resonance in the GHz range (where some assumptions taken analytically are not valid numerically) it is expected that the analytical prediction and numerical calculations to coincide for lower frequencies.

A significant advantage of chiral Swiss rolls, is the fact that their resonant frequency can easily be tuned over a wide range of frequencies (from few MHz to tens of GHz), by simply changing the packing, the radius or the length of the conducting sheet, or the dielectric constant of the material in the gap. Also, chiral Swiss rolls do not require dipole inclusions in order to show a negative band, as the helical conducting wire structure does [10], since their spiral shape ensures a magnetic resonance for waves with a magnetic field parallel to the rod.

Finally, probably the most important advantage of chiral Swiss rolls is the fact that they exhibit extreme chirality compared with other chiral structures discussed in the literature [10, 12], by a factor of at least two orders of magnitude. The measure of this efficiency is their cross section, which is typically (1/100)th to (1/1000)th of the wavelength. Other structures proposed for chiral metamaterials such as the helical structures require a much larger cross section to achieve any significant activity. This is also the main reason that for chiral Swiss rolls a backward wave can be observed even for GHz frequencies, whereas for loop wires or helical wires, it appears for a less broad frequency range or is lost in the stop-band due to sharp resonances [10]. Furthermore, this structure, in addition to magnetic resonance imaging (MRI) applications that are well known [17], is ideal for polarization rotation/selection antenna applications. The extreme chirality of Swiss rolls ensures a tremendous enhancement of the efficiency for these types of antennas, where a linear wave needs to be transformed to a circularly polarized wave [12].

## 4. Conclusion

The prospect of achieving negative refraction using chiral Swiss roll metamaterials is discussed in this paper, where it was found that Swiss rolls exhibit at least 100 times more chirality than other structures previously reported in literature, and therefore ensuring a broader backward wave. A detailed analytical discussion is reported in this paper for the electromagnetic, chiral parameters, and the band structure of a 2D chiral Swiss roll medium, where a significant agreement with numerical calculations was found. Finally, chiral Swiss rolls can be used in antenna applications based on polarization rotation/selection, and due to their extreme chirality to enhance efficiency.

## Appendix. Electromagnetic and chirality parameters of Swiss rolls

Consider uniform fields $H_z$ and $E_z$ applied along a right-handed chiral Swiss roll and assume that:

(i) there are no local field effects giving to the cylinder a rotational symmetry and the current varies only across

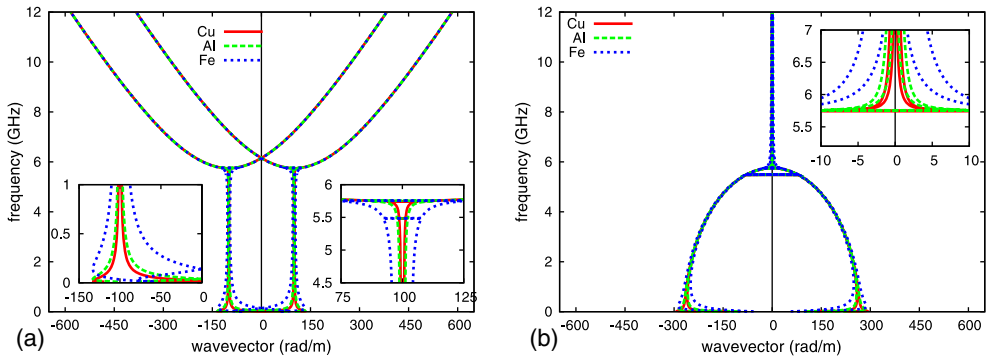


**Figure 9.** The band structure (a) real part, (b) imaginary part of a 2D Swiss roll metamaterial with dimensions $N = 2$, $R = 1$ mm, $l = 5$ mm, $x = 0.05$ mm, $d = 0.35$ mm, $\theta = 21, 7°$ and $a = 5$ mm. Red solid line: Copper–Cu with resistivity $= (1.67 \times 10^{-8})$ Ω m, green dashed lines: aluminium with resistivity $= (2.74 \times 10^{-8})$ Ω m and blue dotted line: Iron–Fe $= (9.8 \times 10^{-8})$ Ω m which is close to the conductivity of germanium.

the width of the conducting sheet. Consequently, only $\mathbf{J_0}$ (figure 4(b)) is driven by *emf*;

(ii) the foil within the dotted lines is not exposed to either the outside or inside of the chiral Swiss roll, and therefore it can be assumed that there is no charge accumulation in this area, and current $\mathbf{J_0}$ is constant in magnitude and direction, written by:

$$\mathbf{J_0} = \mathbf{J_{0x}} \sin\theta + \mathbf{J_{0z}} \cos\theta \tag{A.1}$$

(iii) the number of turns ($N$) is large, ensuring a large overlap of the conducting sheet;

(iv) the current outside the dotted lines rotates until is parallel to the edges of the foil, and therefore the rotation is assumed to be linear with distance;

(v) and finally assume that all fields are of the form $\exp(-\mathrm{i}\omega t)$

Let us consider initially the current flowing through the capacitive elements of the structure. the charge accumulated at the edges of the foil (i.e. outside the dotted lines) needs to be considered, which charges the capacitor created from the overlapping conducting sheet. Therefore, the current across the width of the foil (figure 4(b)) is given by:

$$\mathbf{J_0} = \mathbf{J_{0x}} \sin\theta + \mathbf{J_{0z}} \cos\theta = \frac{\mathrm{d}Q}{\mathrm{d}t} = (N-1)C\frac{\mathrm{d}V}{\mathrm{d}t} \tag{A.2}$$

where $Q$ is the charge accumulated outside of the dotted lines, $V$ is the potential difference between two parallel conducting plates and $C$ is the capacitance per unit length of each exposed turn, given by:

$$C = \frac{\varepsilon_d \varepsilon_0 (\text{width})}{(\text{separation of the plates}) \times (\text{no. of turns})} = \frac{\varepsilon_d \varepsilon_0 2\pi R \sin\theta}{(N-1)d}. \tag{A.3}$$

Since $V$ is of the form $V_0 \exp(-\mathrm{i}\omega t)$, then:

$$\therefore \mathbf{J_{0x}} \sin\theta + \mathbf{J_{0z}} \cos\theta = -\frac{\mathrm{i}\omega\varepsilon_d\varepsilon_0 2\pi R \sin\theta}{d} V. \tag{A.4}$$

Also, the magnetic field along the Swiss roll is given by:

$$H_z = H_0 + J_{0x} - \frac{\pi R^2}{a^2} J_{0x} \tag{A.5}$$

where $H_0$ is the external magnetic field, the second term of the above equation is caused directly by the current flow on the conducting sheet and the last term is due to depolarizing fields with sources at the remote ends of the cylinders. If the cylinders are very long, then the depolarizing field uniformly spreads over the unit cell.

Furthermore, the emf can be calculated by considering $k_y$-propagation and $E_x$-field, ensuring a magnetic field along the $z$-axis, which in its turn induces current that flow around the spiral ring. Using Faraday's law of induction, emf is given by:

$$\mathcal{E} = -(N-1)\frac{\mathrm{d}\Phi}{\mathrm{d}t} = -(N-1)\pi R^2 \mu_0 \frac{\mathrm{d}H_z}{\mathrm{d}t}. \tag{A.6}$$

$\mathcal{E}$ needs to be balanced by the ohmic drop in the potential ($V$) due to the capacitance of the structure and conductivity losses ($=2\pi R(N-1)\rho J_{ox}$), therefore:

$$\therefore \mathrm{i}\omega(N-1)\pi R^2 \mu_0 H_z = V + 2\pi R(N-1)\rho J_{0x} \tag{A.7}$$

where $\rho$ is the resistance of the conducting sheet per unit length.

Finally, the potential difference ($V$) across $(N-1)$ conducting sheets can be calculated by integrating around a loop in the $y$–$z$ plane of the structure, giving:

$$V = \int E\,\mathrm{d}x = (E_0 + E_\mathrm{p})(N-1)2\pi R \tan\theta \tag{A.8}$$

where $E_\mathrm{p}$ is the electric field driven by the current per unit length of the circumference of the coil, which is induced by charge accumulation. Therefore $E_\mathrm{p} = [\frac{2\pi R}{\mathrm{i}\omega\varepsilon_d\varepsilon_0 a^2} - p]J_{0z}$ and

$$E_0 + E_\mathrm{p} = E_0 + \left[\frac{2\pi R}{\mathrm{i}\omega\varepsilon_d\varepsilon_0 a^2} - p\right] J_{0z} = \frac{V}{(N-1)2\pi R \tan\theta}. \tag{A.9}$$

Now, solving (A.4), (A.5), (A.7) and (A.9) with respect to $J_{0x}$ and $J_{0z}$:

$$J_{0x} = \frac{-[AL\tan^2\theta + B]\omega^2 H_0 - C\omega\tan\theta E_0}{\omega^2 D(AL\tan^2\theta + B) + \omega(KL\tan^2\theta + C\rho) - L\tan^2\theta} \tag{A.10}$$

$$J_{0z} = -\frac{B\omega^2}{L\tan\theta}H_0 + \left(\frac{BD\omega^2 + C\rho\omega}{L\tan\theta}\right) \times \frac{[AL\tan^2\theta + B]\omega^2 H_0 + C\omega\tan\theta E_0}{\omega^2 D(AL\tan^2\theta + B) + \omega(KL\tan^2\theta + C\rho) - L\tan^2\theta} - \frac{C\omega}{L}E_0 \tag{A.11}$$

where

$$A = \frac{2\pi^2 R^3 \varepsilon_d (N-1)}{d c_0^2} \qquad B = \frac{\varepsilon_d a^2}{4\pi c_0^2}$$
$$C = \frac{\mathrm{i}\varepsilon_d\varepsilon_0 a^2}{2\pi R} \qquad D = 1 - \frac{\pi R^2}{a^2} = 1 - F \tag{A.12}$$
$$K = \frac{\mathrm{i}\varepsilon_d\varepsilon_0 4\pi^2 R^2 \rho (N-1)}{d}$$
$$L = 1 - C\rho\omega \tag{A.13}$$

and where $F$ is the filling factor and $F = \frac{\pi R^2}{a^2}$ and $\rho$ is the resistance of the roll per unit area.

Finally, since the average $H$-field is given by the sum of $H_0$ and the depolarizing fields from the coils $H_\mathrm{ave} = H_0 - J_{0x}\frac{\pi R^2}{a^2}$ and $\mu = B_\mathrm{ave}/(\mu_0 H_\mathrm{ave})$ then $\chi_{HH}$, $\chi_{HE}$ are given by:

$$[\chi^{-1}]_{HH} = \frac{1}{(1-F)}\frac{\omega^2 - \omega_0^2 + \mathrm{i}\Gamma\omega}{\omega^2 - \omega_\mathrm{mp}^2 + \mathrm{i}\Gamma\omega/D} \tag{A.14}$$

$$[\chi^{-1}]_{HE}/\varepsilon_0 = \frac{\mathrm{i}R}{2L\tan\theta}\left(\frac{\omega_\mathrm{mp}^2\omega}{\omega^2 - \omega_\mathrm{mp}^2 + \mathrm{i}\Gamma\omega/D}\right) = [\kappa^{-1}]_{HE} \tag{A.15}$$

where

$$\omega_0^2 = \frac{L\tan^2\theta}{AL\tan^2\theta + B} = \frac{\tan^2\theta}{\varepsilon_d\left(\frac{2\pi^2R^3(N-1)}{dc_0^2}\tan^2\theta + \frac{a^2}{4\pi c_0^2}\right)} \tag{A.16}$$

$$\omega_\mathrm{mp}^2 = \frac{L\tan^2\theta}{D(AL\tan^2\theta + B)} = \frac{\tan^2\theta}{\varepsilon_d\left(1 - \frac{\pi R^2}{a^2}\right)\left(\frac{2\pi^2R^3(N-1)}{dc_0^2}\tan^2\theta + \frac{a^2}{4\pi c_0^2}\right)} = \frac{\omega_0^2}{1-F} \tag{A.17}$$

are the resonant and the magnetic plasma frequencies respectively and

$$\Gamma = -\mathrm{i}\frac{(KL\tan^2\theta + C\rho)}{AL\tan^2\theta + B} = -\frac{2\rho}{\mu_0 R}. \tag{A.18}$$

Similarly for $\varepsilon$, $\chi_{EE}$ and $\chi_{EH}$ are given by:

$$[\chi^{-1}]_{EE} = G\left(\frac{\omega^2 - \mathrm{i}\omega\Gamma/D}{\omega^2 - \omega_\mathrm{p}^2 - \mathrm{i}\omega\Gamma/D}\right) \tag{A.19}$$

where $G$ is a constant given by:

$$G = \frac{B}{L(A\tan^2\theta + B)} = \frac{\frac{a^2}{4\pi c_0^2}}{L(\frac{2\pi^2R^3(N-1)}{dc_0^2}\tan^2\theta + \frac{a^2}{4\pi c_0^2})}$$
$$= \frac{a^2 d}{L(8\pi^3R^3(N-1)\tan^2\theta + a^2 d)} \tag{A.20}$$

and

$$\omega_\mathrm{p} = \omega_\mathrm{mp} \tag{A.21}$$

are the plasma frequency, and finally:

$$[\chi^{-1}]_{EH}/\mu_0 = -\frac{\mathrm{i}R}{2L\tan\theta}\left(\frac{\omega\omega_\mathrm{mp}^2}{\omega^2 - \omega_\mathrm{mp}^2 - \mathrm{i}\Gamma\omega/D}\right)$$
$$= [\kappa^{-1}]_{EH}. \tag{A.22}$$

## References


[1] Veselago V G 1968 The electrodynamics of substances with simultaneously negative values of $\varepsilon$ and $\mu$ *Sov. Phys.—Ups.* **10** 509

[2] Pendry J B, Holden A J, Stewart W J and Young I 1996 Extremely low frequency plasmons in metallic mesostructures *Phys. Rev. Lett.* **76** 4773–6

[3] Pendry J B, Holden A J, Robbins D J and Stewart W J 1998 Low frequency plasmons in thin-wire structures *J. Phys.: Condens. Matter* **10** 4785–809

[4] Demetriadou A and Pendry J B 2008 Taming spatial dispersion in wire metamaterial *J. Phys.: Condens. Matter* **20** 295222

[5] Pendry J B, Holden A J, Robbins D J and Stewart W J 1999 Magnetism form conductors and enhanced nonlinear phenomena *IEEE Tran. Microw. Theory Tech.* **47** 2075

[6] Pendry J B 2004 A chiral route to negative refraction *Science* **306** 1353–5

[7] Potts A, Papakostas A, Bagnall D M and Zheludev N I 2004 Planar chiral meta-materials for optical applications *Microelectron. Eng.* **73/74** 367–71

[8] Plum E, Fedotov V A, Schwanecke A S, Zheludev N I and Chen Y 2007 Giant optical gyrotropy due to electromagnetic coupling *Appl. Phys. Lett.* **90** 223113

[9] Rogacheva A V, Fedotov V A, Schwanecke A S and Zheludev N I 2006 Giant gyrotropy due to electromagnetic-field coupling in a bilayered chiral structure *Phys. Rev. Lett.* **97** 177401

[10] Tretyakov S, Sihvola A and Jylha L 2005 Backward-wave regime and negative refraction in chiral composites *Photon. Nanostruct. Fundam. Appl.* **3** 107–15

[11] Sihvola A 2007 Metamaterials in electromagnetics *Metamaterials* **1** 2–11

[12] Silveirinha M G 2008 Design of linear-to-circular polarization transformers made of long densely packed metallic helices *IEEE Trans. Antennas Propag.* **56** 390–401

[13] Ramakrishna S A 2005 Physics of negative refractive index materials *Rep. Prog. Phys.* **68** 449

[14] Wiltshire M C K 2007 Radio frequency (rf) metamaterials *Phys. Status Solidi* **244** 1227–36

[15] Wiltshire M C K, Hajnal J V, Pendry J B, Edwards D J and Stevens C J 2003 Metamaterial endoscope for magnetic field transfer: near field imaging with magnetic wires *Opt. Express* **11** 709–15

[16] Demetriadou A and Pendry J B 2009 Numerical analysis of Swiss roll metamaterial *J. Phys.: Condens. Matter* **21** 326006

[17] Wiltshire M C K, Pendry J B and Hajnal1 J V 2006 Sub-wavelength imaging at radio frequency *J. Phys.: Condens. Matter* **19** 456216